Proceedings of the 2016 International Mechanical Engineering Congress & Exposition
IMECE2016
November 11-17, 2016, Phoenix, Arizona, USA

IMECE2016-68197

EFFICIENT MODELING OF NONLINEAR SCATTERING OF ULTRASONIC GUIDED WAVES FROM FATIGUE CRACKS USING LOCAL INTERACTION SIMULATION APPROACH

Yanfeng Shen
UM-SJTU Joint Institute
Shanghai Jiao Tong University
Shanghai, China

Carlos E.S. Cesnik
Department of Aerospace Engineering
University of Michigan
Ann Arbor, Michigan, USA

ABSTRACT

This paper presents an efficient modeling technique to study the nonlinear scattering of ultrasonic guided waves from fatigue damage. A Local Interaction Simulation Approach (LISA) is adopted, which possesses the versatility to capture arbitrary fatigue crack shapes. The stick-slip contact dynamics is implemented in the LISA model via the penalty method, which captures the nonlinear interactions between guided waves and fatigue cracks. The LISA framework achieves remarkable computation efficiency with its parallel implementation using Compute Unified Device Architecture (CUDA) executed on GPUs. A small-size LISA model is tailored for the purpose of extracting the guided wave scattering features. The model consists of an interior damage region and an exterior absorbing boundary. The interior damage region captures various types of fatigue crack scenarios, while the exterior absorbing boundary surrounds the damage model to eliminate boundary reflections. Thus, the simulation of guided wave scattering in an infinite media can be achieved utilizing a small-size local LISA model. Due to the parallel CUDA implementation and the small-size nature, this local LISA model is highly efficient. Selective mode generation is achieved by coupling/decoupling excitation profiles with certain wave mode shapes, which allows the study of sensitivity of different wave modes to a certain fatigue damage situation. At the sensing locations, mode decomposition is performed on the scattering waves, which enables the study of mode conversion at the damage. Fourier analysis allows the extraction of scattering features at both fundamental and higher harmonic frequencies. A numerical case study on nonlinear scattering of guided waves from a fatigue crack is given. The higher harmonic generation and mode conversion phenomena are presented using the wave damage interaction coefficients (WDIC), from which the sensitive detection directions can be inferred to place sensors. This study can provide guidelines for the effective design of sensitive SHM systems using nonlinear ultrasonic guided waves for fatigue crack detection.

INTRODUCTION

Guided-wave Structural Health Monitoring (SHM) systems generally identify damage by detecting the scattering waves. The effectiveness and sensitivity of an SHM sensor array depends on whether the sensors can receive sufficient damage-scattered wave energy at the sensing locations. Thus, it is important to understand the scattering features of ultrasonic guided waves from structural damage such as wave mode sensitivity, interrogation frequency influence, scattering amplitude and directionality, mode conversion effects, etc. Nonlinear ultrasonic techniques are drawing increasing attention in SHM applications due to their sensitivity to incipient fatigue cracks in structures. However, the nonlinear scattering features are quite complex with distinctive phenomena such as harmonic generation and mode conversion.

The fundamentals of wave damage interaction have been investigated analytically. Approximate solutions using Kirchhoff, Mindlin, Kane-Mindlin plate theory have been reported in the literature [1]. Moreau et al. applied 3D elasticity solution or exact Lamb wave solution to solve the wave scattering problem from cavities and flat-bottomed damage with irregular shapes [2]. Although these analytical methods manage to offer fast parametric studies, they are only possible for simple damage types. To solve guided wave scattering from arbitrary damage, Moreau et al. further developed small-size local finite element models (FEM) with absorbing boundaries [3]. Such local FEM can provide efficient predictive results of wave scattering from complex structural damage due to its light computational burden and frequency domain harmonic solution scheme. This technique has been used to provide the wave damage interaction information for the analytical wave

propagation solution, forming a combined global analytical local FEM approach to simulate guided wave damage detection [4]. However, the state of the art generally focused on linear scattering phenomena; the investigation of nonlinear scattering and mode conversion at fatigue cracks is still very limited. And the solution to such contact acoustic nonlinearity (CAN) problem is only possible via time domain transient analysis. Although nonlinear interaction between guided waves and breathing cracks have been attempted using FEM contact analysis, the implicit nonlinear solution scheme imposes much computational burden during the analysis [5].

This study investigates the nonlinear scattering phenomena at fatigue cracks using a small-size numerical model with a normal mode decomposition technique. Local Interaction Simulation Approach (LISA) is adopted to construct the numerical model. The contact LISA model follows an explicit solving scheme and is parallelized by Compute Unified Device Architecture (CUDA) executed on GPUs with two orders of magnitude higher computational efficiency compared with nonlinear FEM solutions [11]. It enables the extraction of wave scattering features of each plate guided wave mode at both fundamental and higher harmonic frequencies.

LOCAL INTERACTION SIMULATION APPROACH WITH CONTACT ACOUSTIC NONLINEARITY

Local Interaction Simulation Approach

LISA is a finite-difference based numerical simulation method. It approximates the partial differential elastodynamic wave equations with finite difference quotients in the discretized temporal and spatial domains. The coefficients in LISA iterative equations (IEs) depend only on the local physical material properties. The Sharp Interface Model (SIM) enforces the stress and displacement continuity between the neighboring computational cells and nodes. Therefore, changes of material properties in the cells surrounding a computational node can be captured through these coefficients. The final iterative equations determine the displacements of a certain node at current time step based on the displacements of its eighteen neighboring nodes at previous two time steps. For details of the derivation for the LISA equations, the readers are referred to Ref. [6]. During the past decade, LISA underwent considerable progress, with its extension to general anisotropic materials [6], coupled field capabilities [7], hybridization with other numerical methods [8, 9], and parallel execution on powerful graphics cards with CUDA technology [10].

Adding Contact Dynamics into LISA

A penalty method is deployed to introduce contact dynamics into LISA. Penalty method is initially investigated to solve a class of constrained optimization problems and have been adopted as one of the primary approaches to simulate contact problems in FEM. It approximates a constrained problem by an unconstrained one whose solution ideally converges to the solution of the original constrained problem. Its convergence is achieved by punishing the violation of these constrains.

For contact analysis, the impenetrability condition in contact continuum mechanics is weakened, which means a small amount of penetration is allowed to enable the mathematical formulation. This penetration can be easily identified as the measurement of violation against the impenetrability condition and is penalized by introducing a contact stiffness that tends to minimize this violation. When an appropriate contact stiffness is reached, the amount of penetration approaches zero, which makes the numerical solution converges towards the physical contact phenomena.

A typical contact procedure during wave crack interaction can be categorized into four consecutive stages: (1) pre-contact state, where the contact surfaces are separate from each other and are subjected to free boundary conditions; (2) contact initiation, where contact counterparts meet, which triggers the exertion of contact forces; (3) in-contact motion, where the crack surface moves together in a stick-slip pattern, with interactive contact forces; (4) contact pair separation, where the contact counterparts leave each other, releasing the contact interactions and regaining the free boundary conditions. It can be noticed that the boundary condition of the contact surfaces alters between free and constrained situations.

To satisfy the alternating boundary conditions at the contact surfaces, special design and treatment of the computational grid are needed. In this study, a discontinuous mesh is used to model the crack surfaces. The structural discretization was carried out using the commercial FEM software ANSYS 14. Then, a model converter was programed using CUDA C to convert the nodal connectivity and material allocation from the FEM format to that of the LISA one. During such conversion procedure, three additional steps were taken to prepare the LISA computational grid for the contact analysis, including contact pair recognition, normal direction detection, and auxiliary air cell addition. Figure 1a shows the discontinuous mesh with separate nodes along the contact surface. A pair of nodes located on the counterpart of the crack surface is designated as a contact pair. The contact forces will be acted interactively on the contact pair nodes. Figure 1b shows a generic contact node and its normal direction with respect to the contact surface. It should be noted that since LISA uses a structured mesh, there will be six normal directions appearing in each contact pair, i.e., +x, -x, +y, -y, +z, -z. In practice, curved surfaces can be approximated by fitting the structured mesh to the target geometry using dense discretization. Figure 1c illustrates the addition of auxiliary air cells to the LISA computational grid surrounding the contact nodes to satisfy a free boundary condition when the crack surfaces are separate from each other and immersed in air. It can be seen that five auxiliary nodes and four air cells are added to each contact node. One may notice that by adding the auxiliary cells, a special contact surface node is brought to the unified LISA computation representation with eighteen neighboring nodes. It should be also noted that the air cells on the contact surfaces are not implemented during structural

discretization in ANSYS but are generated during the model conversion procedure. When the crack surfaces come into contact, penalty contact forces are acted on the contact nodes to constrain the in-contact motion. In this way, the modeling of the alternating boundary condition can be achieved.

The contact forces at each contact pair are computed based on the penalty formulation for each time step. A Coulomb friction model is integrated to simulate stick-slip contact motion. The details of the nonlinear contact LISA formulation can be found in Ref [11].

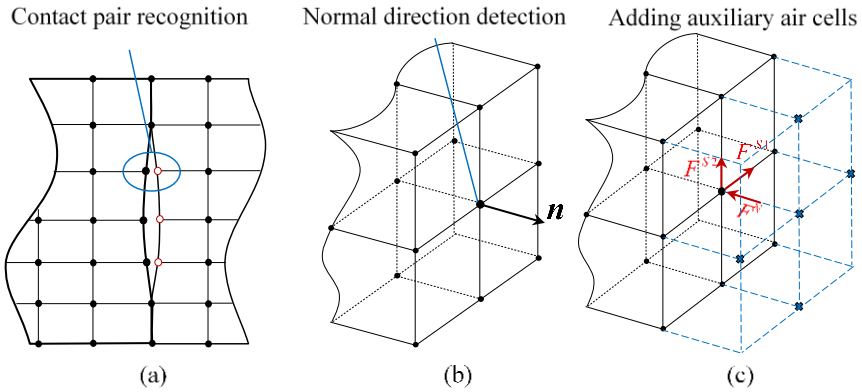

Figure 1: Special treatment on the computational grid to introduce contact dynamics in LISA: (a) contact pair recognition; (b) normal direction detection; (c) auxiliary air cells addition

Numerical Implementation Using CUDA

In this study, the contact LISA algorithm was implemented using CUDA technology and executed in parallel on GPUs (NVIDIA GeForce Titan with 2688 CUDA cores and 28672 concurrent threads). There are two major characteristics of the current contact LISA formulation that enables the computation to be expedited. First, LISA is massively parallel. This is because the computation of a general node or a contact node only depends on the solutions of its eighteen neighboring nodes at the previous two time steps. Thus, the behavior of each node is independent from the others at the target time step, i.e., the computation of each node can be carried out individually in parallel. Second, the wave propagation simulation tasks usually require dense discretization of the structure, resulting in a computationally intensive problem. GPUs, with their massive concurrent thread feature, are suitable to handle such large size problems by distributing the workloads among a large number of functional units and carry out highly efficient parallel computing. During the computation, the parameters are first established in the host memory (RAM). Then a copy of these parameters is sent to the device memory (GPU global memory) for it to be processed. The computation of each node is assigned to a functional thread, i.e., each thread gathers the displacements of its eighteen neighboring nodes and one contact pair node (if identified as a contact node) at previous two time steps, process the material properties in the eight surrounding cells, and execute the kernel to compute the displacements of this node at the target time step. Since one of the bottlenecks of a CUDA program is the data transfer between the device memory and host memory, results are transferred from the GPU to the CPU only sporadically (every 10-30 steps depending on the frequency of the propagating waves) to minimize such data transfer cost.

SMALL-SIZE LISA MODEL FOR STUDYING WAVE DAMAGE INTERACTIONS

LISA Model

Figure 2 shows the small-size LISA model used in this study for investigating wave damage interactions. The model consists of an interior damage region and an exterior absorbing boundary. The interior damage region is able to capture arbitrary damage scenarios, while the exterior absorbing boundary surrounds the damage model to eliminate boundary reflections. For this particular study, Absorbing Layers using Increasing Damping (ALID) method is applied to implement the non-reflective boundary. Thus, the simulation of guided wave scattering in an infinite plate can be achieved utilizing the small-size local LISA model. In general, the extended ALID region should be longer than twice the longest wave length under consideration [12, 13].

The red circle in the model shows the incident wave excitation locations, while the blue circle represents the scattering wave sensing locations. The circular-shape locations allow the investigation of scattered waves in any direction β from an incident wave with any incident angle α. At the wave generation locations, circular areas of out-of-plane traction forces are applied on both top and bottom surfaces of the plate. Anti-phase traction force pairs will generate symmetric Lamb wave mode (S0) and in-phase traction force pairs will generate

anti-symmetric Lamb wave mode (A0). At the sensing locations, for each scattering direction β, a number of sensing points across the thickness at locations Z_i are obtained for mode decomposition analysis.

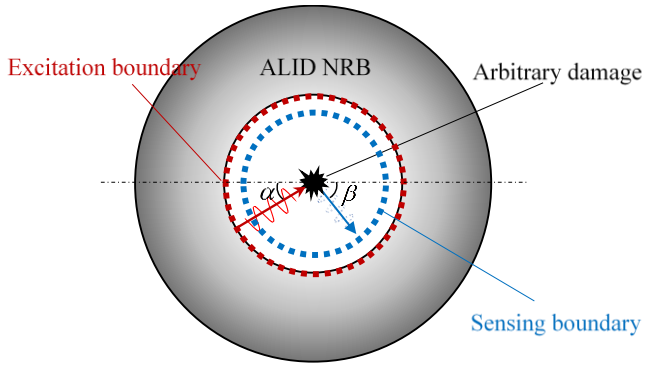

Figure 2: Small-size LISA model with non-reflective boundary for studying wave damage interactions

To obtain the scattered wave information, a pair of such small-size LISA model is needed: one pristine case and one damaged case. The pristine case model provides the wave field of the incident waves, while the damaged case mode gives the wave filed of the total waves, the superposition of incident waves and scattered waves. The subtraction of incident waves from the total wave field renders the scattered wave field. The LISA models used in this study adopts the in-plane cell size of 1 mm and a through-thickness cell size of 0.5 mm. The time step according to the Courant-Friedrichs-Lewy (CFL) condition is 64.75 ns, which corresponds to a CFL number of 0.99.

Simulation Example

Figure 3 shows the case example of simulation results for the nonlinear interactions between guided waves and 2-cm long through-thickness fatigue crack in a 5-mm thick aluminum plate. This case simulates the perpendicular incidence of guided waves with the straight line crack. Selective S0 and A0 Lamb modes are generated by continuous harmonic surface traction forces at 250 kHz. To accommodate all the possible wave modes participating in the scattering procedure, the model size is set to be 100 mm in radius. And the wave generation location is 50 mm away from the fatigue crack at the center of the model. The sensing circle has a radius of 40 mm (8 times the plate thickness), which allows the complete development of wave modes (including evanescent modes). Thus, at the sensing locations, only propagating modes meaningful for SHM systems will be picked up. The absorbing region extends from the excitation locations with a length of 50 mm.

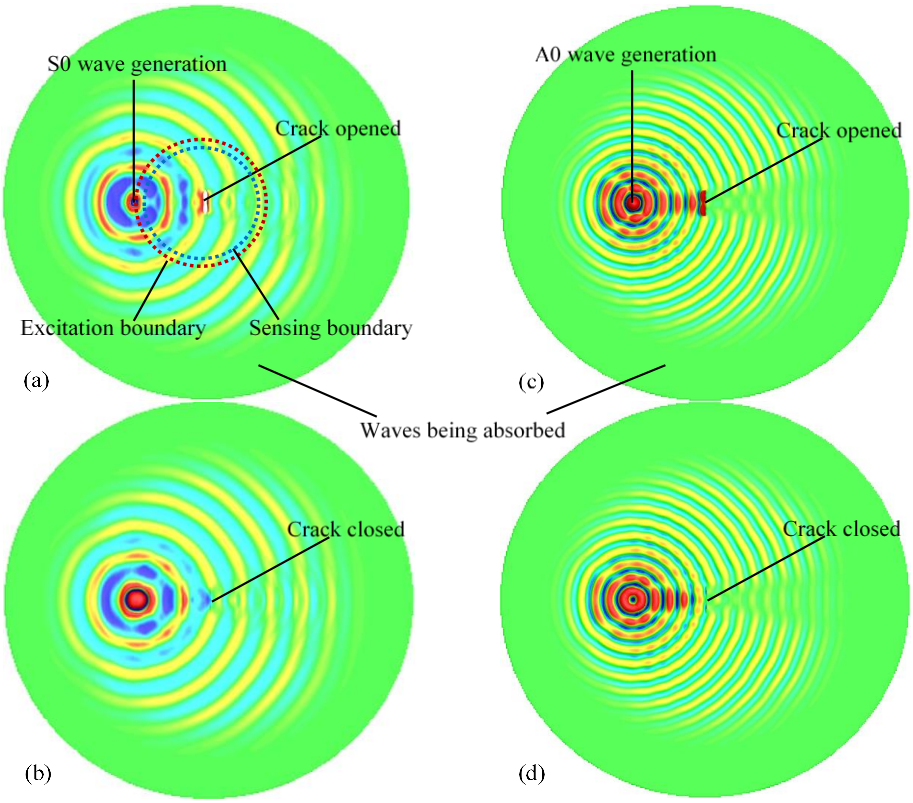

Figure 3: Small-size LISA model simulation result: (a) S0 wave opened the crack; (b) S0 wave closed the crack; (c) A0 wave opened the crack; (d) A0 wave closed the crack

The left column of Figure 3 presents S0 wave interaction with the fatigue crack, while the right column shows A0 wave interaction with the fatigue crack. The top row of Figure 3 presents the crack being opened by the incident waves, while the bottom row shows the crack being closed by the incident waves. Such crack open-close contact-impact mechanism gives rise to the nonlinearity in the sensing signals. It can be noticed that the waves entered the ALID NRB region are effectively absorbed.

Figure 4a shows the time trace of the excitation signal. A half Hanning window is applied on the continuous harmonic sine wave to smoothly introduce guided waves into the dynamic system. Figure 4b presents the frequency spectrum of the excitation signal with only one component f_c at the fundamental excitation frequency (250 kHz). Figure 4c shows the out-of-plane component u_Z of the scattered wave signal during S0 wave interaction with the fatigue crack. The scattered signal is heavily distorted with obvious zigzag shapes. Figure 4d presents the frequency spectrum of the scattered wave signal. It can be observed that in addition to the fundamental frequency f_c, distinctive higher harmonic components at $2f_c$ and $3f_c$ are present. Such nonlinear higher harmonic components bring complexity in analyzing the scattered wave components. This will be further discussed in the next section.

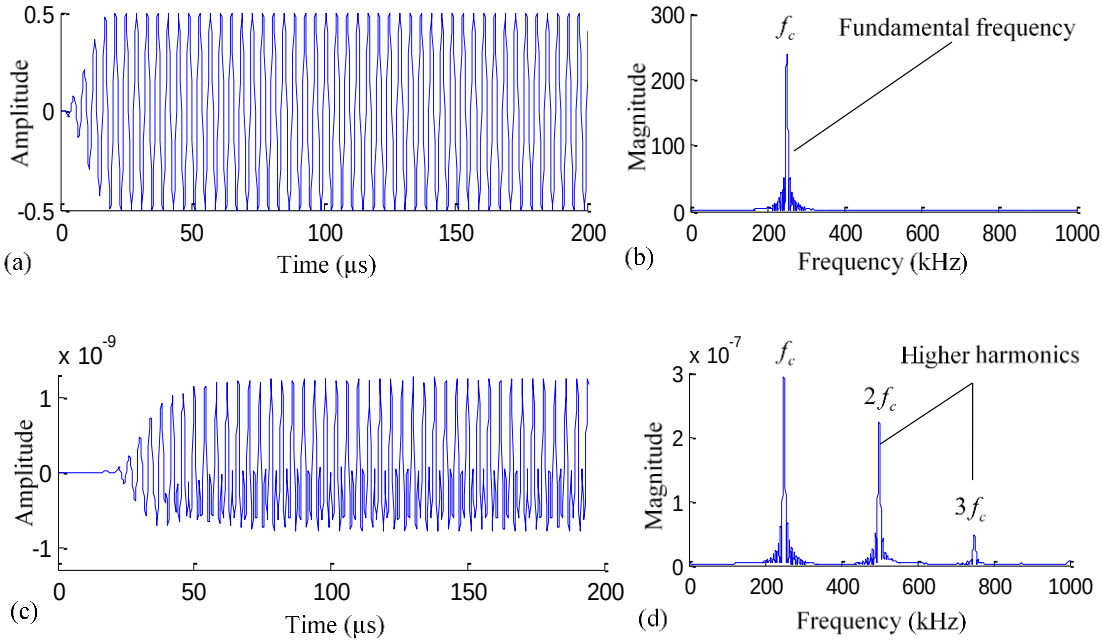

Figure 4: Signal examples: (a) time trace of excitation signal; (b) frequency spectrum of excitation signal; (c) time trace of scattered signal; (d) frequency spectrum of scattered signal

FORMULATION FOR QUANTITATIVE EVALUATION OF SCATTERED WAVE MODES

Challenge from Multi-modal Plate Guided Waves

In addition to the CAN simulation, another major challenge for quantitatively analyzing nonlinear scattering wave modes stems from the multi-modal feature of plate guided waves. As shown in Figure 4, the scattered waves not only contain the fundamental excitation frequency but also higher harmonic components. For the case of 250-kHz excitation, the scattered waves have 250 kHz, 500 kHz, 750 kHz, etc. These higher harmonic frequencies will inevitably bring in increasing number of higher Lamb modes when higher harmonics appear beyond corresponding cut-off frequencies. The increasing number of wave modes will result in multiplex possibilities of mode conversions.

Figure 5 shows the dispersion curves of a 5-mm thick aluminum plate guided waves. In order to capture the scattering wave features, all the plate guided wave modes should be considered in the scattering analysis, because one incident wave mode may be converted to all possible Lamb modes and shear horizontal (SH) modes. It can be observed that at f_c (250 kHz) there are three possible wave modes: A0, SH-S0, and S0. Thus, a certain type of incident wave mode can be converted to any of these three wave modes after interacting with the damage. However, at $2f_c$ (500 kHz), there are five possible wave modes: the three fundamental modes (A0, SH-S0, S0) and

two higher-order modes (SH-A0 and A1). Thus, one incident wave mode may be converted into all these five possible wave modes. Figure 5 also presents the five plate wave mode shapes at the second harmonic frequency. These mode shapes will be used to achieve the mode decomposition for the quantitate evaluation of scattered waves.

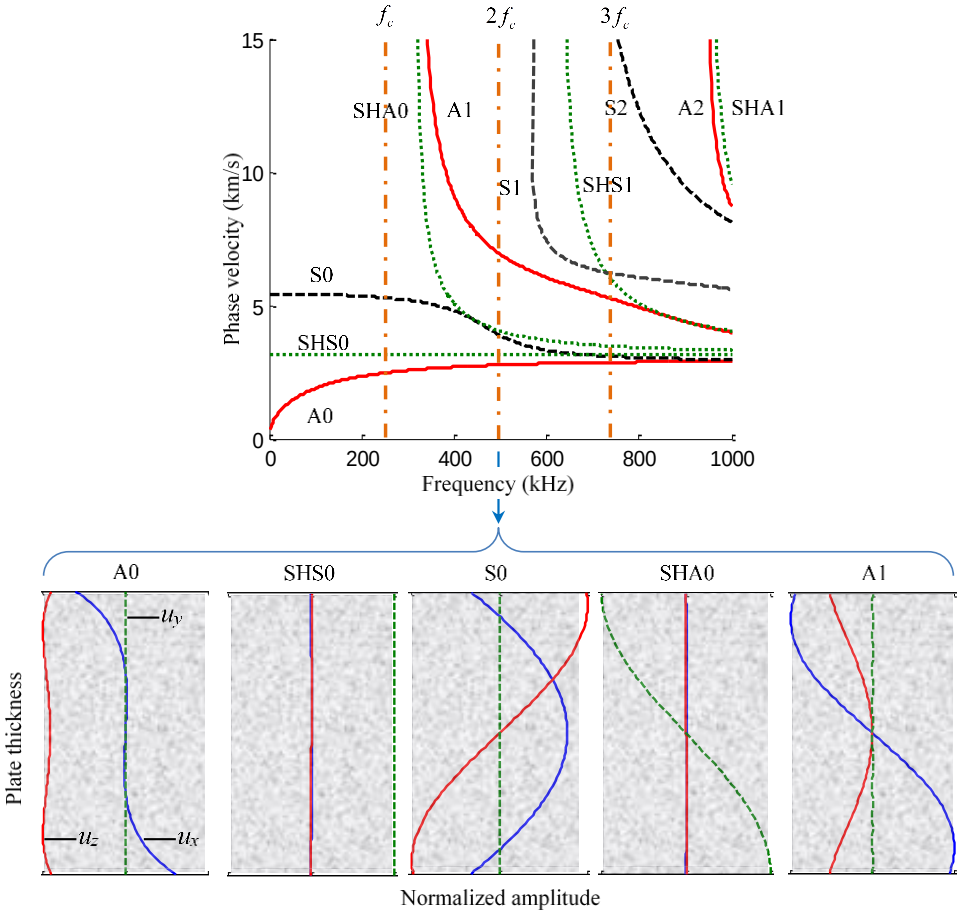

Figure 5: Multi-modal Lamb waves and their mode shapes at second harmonic frequency for a 5-mm thick aluminum plate

Wave Damage Interaction Coefficients Extraction

The quantitative participation of each wave mode in the scattered wave field is represented by the wave damage interaction coefficients (WDICs) $C_{IN-N}(\alpha,\beta,f_n)$. The two sub-indices are used to designate the incident wave mode and the scattered wave mode, respectively. α and β are the incident angle and scattered direction. f_n represents the harmonic frequency component, i.e., f_1 represents fundamental excitation frequency, while f_2 and f_3 represents second and third higher harmonic frequencies, respectively. For instance, $C_{S0-SHS0}(20,30,f_2)$ represents the second harmonic scattering coefficient of S0 wave with 20° incident angle and mode converted to SHS0 in the 30° scattered direction.

The extraction of WDICs from the small-size LISA model can be realized in the following steps:

STEP 1: after the computation of a pristine case (incident wave field u_{IN}) and a damaged case (total wave field u_{Total}), the scattered wave field is obtained by

$$u_{SC} = u_{Total} - u_{IN} \tag{1}$$

STEP 2: the scattered wave field at the sensing boundary is converted into cylindrical coordinate system shown in Figure 6 through coordinate transformation. $u_r(\beta,t,Z_i)$, $u_\theta(\beta,t,Z_i)$, and $u_z(\beta,t,Z_i)$ represent the cylindrical coordinate displacements of the scattered wave field at various thickness locations Z_i in the scattering direction β. It should be noted that in the pristine case, an additional center sensing node is

used. The displacements in the center of the model are recorded as the incident wave field impinging on the damage location $u_{IN}^{Center}(\alpha,t)$.

STEP 3: both the incident wave at the damage location and the scattered wave are Fourier transformed into frequency domain.

$$U_{SC}^{LISA}(\beta, f_n, Z_i) = FFT\left[u_{SC}^{LISA}(\beta,t,Z_i)\right] \tag{2}$$

$$U_{IN}^{Center}(\alpha, f_1) = FFT\left[u_{IN}^{Center}(\alpha,t)\right] \tag{3}$$

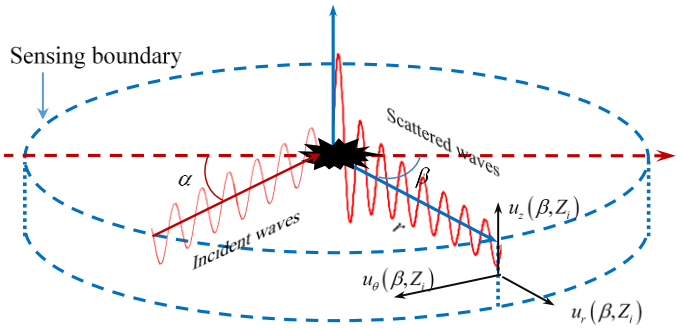

Figure 6: Cylindrical coordinate system and the sensing points in different scattering directions and across the plate thickness

STEP 4: consider the waves irradiating from a localized location follows the solution of Hankel functions [14]. The wave scattering formulation can be written as

$$\sum_N u_{IN}^{Center}(\alpha, f_1)\cdot C_{IN-N}(\alpha,\beta, f_n)\cdot \phi_N(f_n,Z_i)\cdot H_m^{(1)}(\xi_N r) = U_{SC}^{LISA}(\beta, f_n, Z_i) \tag{4}$$

where ξ_N is the frequency dependent wavenumber of wave mode N; $\phi_N(f_n,Z_i)$ represents the corresponding mode shapes at harmonic frequency f_n at the thickness location Z_i. $H_m^{(1)}$ is the Hankel function of the first kind and order m. When the scattered wave mode is Lamb wave, $m=1$; when the scattered wave mode is SH wave, $m=0$. r is the distance between the center of the model and the sensing boundary. The physical interpretation of Eq. (4) is that the waves impinging the damage is modified by the WDICs governing the participation of each scattered wave mode. These scattered waves carry their mode shapes, undergo an out-spreading propagation, and finally arrive at the sensing boundary.

The incident wave $u_{IN}^{Center}(\alpha, f_1)$ and scattered sensing signals $U_{SC}^{LISA}(\beta, f_n, Z_i)$ have been obtained as complex numbers from the Fourier transform. The mode shapes $\phi_N(f_n,Z_i)$ and wavenumbers ξ_N can be obtained from either the analytical solution or the Semi-analytical Finite Element (SAFE) method. The only unknown terms in Eq. (4) are the WDICs. Note that Eq. (4) will provide an independent equation for each sensing node for each coordinate direction. For instance, if n nodes across the thickness are used, then a total of $3n$ equations will be obtained for a certain scattering direction. In the end, one arrives at an over-determined system of equations with fixed number of unknown WDICs for a certain frequency and a large number of equations depending on the number of solutions used across the thickness.

STEP 5: Eq. (4) is casted into matrix form and solved using the least square method, i.e.,

$$\Phi_{3n\times N}\cdot H_{N\times N}\cdot C_{N\times 1} = \frac{1}{U_{IN}^{Center}} U_{SC\_3n\times 1}^{LISA} \tag{5}$$

where Φ is the mode shape matrix; H is the Hankel function diagonal matrix; C is the WDIC vector; U_{SC}^{LISA} is the LISA solution vector. These matrices are given as:

$$\Phi = \begin{bmatrix} \phi_1^r(Z_1) & \phi_2^r(Z_1) & \cdots & \phi_N^r(Z_1) \\ \vdots & & & \vdots \\ \phi_1^r(Z_i) & \phi_2^r(Z_i) & \cdots & \phi_N^r(Z_i) \\ \phi_1^\theta(Z_1) & \phi_2^\theta(Z_1) & \cdots & \phi_N^\theta(Z_1) \\ \vdots & & & \vdots \\ \phi_1^\theta(Z_i) & \phi_2^\theta(Z_i) & \cdots & \phi_N^\theta(Z_i) \\ \phi_1^z(Z_1) & \phi_2^z(Z_1) & \cdots & \phi_N^z(Z_1) \\ \vdots & \vdots & & \vdots \\ \phi_1^z(Z_i) & \phi_2^z(Z_i) & \cdots & \phi_N^z(Z_i) \end{bmatrix} \tag{6}$$

$$H = \begin{bmatrix} H_m^{(1)}(\xi_1 r) & 0 & \cdots & 0 \\ 0 & H_m^{(1)}(\xi_2 r) & 0 & \vdots \\ \vdots & 0 & \vdots & 0 \\ 0 & \cdots & 0 & H_m^{(1)}(\xi_N r) \end{bmatrix} \tag{7}$$

$$C = \begin{bmatrix} C_1 & C_2 & \cdots & C_N \end{bmatrix}^T \tag{8}$$

$$U_{SC}^{LISA} = \left[U_r^{LISA}(Z_{1\to i}) \quad U_\theta^{LISA}(Z_{1\to i}) \quad U_z^{LISA}(Z_{1\to i})\right]^T \tag{9}$$

The solution of Eq. (5) is conducted for each scattering direction and the final direction-dependent scattering WDICs are obtained. The WDICs are complex-valued coefficients which contain corresponding amplitude and phase information. The phase coefficients are evaluated in $[0, 2\pi]$.

CASE STUDY: NONLINEAR SCATTERING AND MODE CONVERSION COEFFICIENTS OF GUIDED WAVES AT A FATIGUE CRACK

This section presents the WDIC results for the 5-mm thick aluminum plate with a 2-cm long fatigue crack. The study focuses on two fundamental incident wave modes: S0 and A0, both coming perpendicular to the crack surfaces ($\alpha = 0$).

S0 Wave Nonlinear Scattering

Figure 7 shows the WDICs for the S0 incident wave at the fundamental frequency f_1 (250 kHz). The top row presents the amplitude coefficients, while the bottom row presents the phase coefficients. At the excitation frequency, only three fundamental wave modes exist. After interacting with the fatigue crack, the S0 wave is not converted to A0 mode, since the WDIC of C_{S0-A0} has an order of magnitude around 10^{-10} and the irregular pattern is attributed to numerical noise. The S0 wave is scattered in its own mode type as shown by the C_{S0-S0} coefficient. Along the incident direction, the scattered S0 wave has the largest amplitude, which indicates that to detect the scattered wave, the most effective location to place the sensors is along the wave path. Mode conversion takes place between the incident S0 mode and the scattered SHS0 mode. The highest SHS0 scattering amplitude peaks appear around ±25° and ±60°.

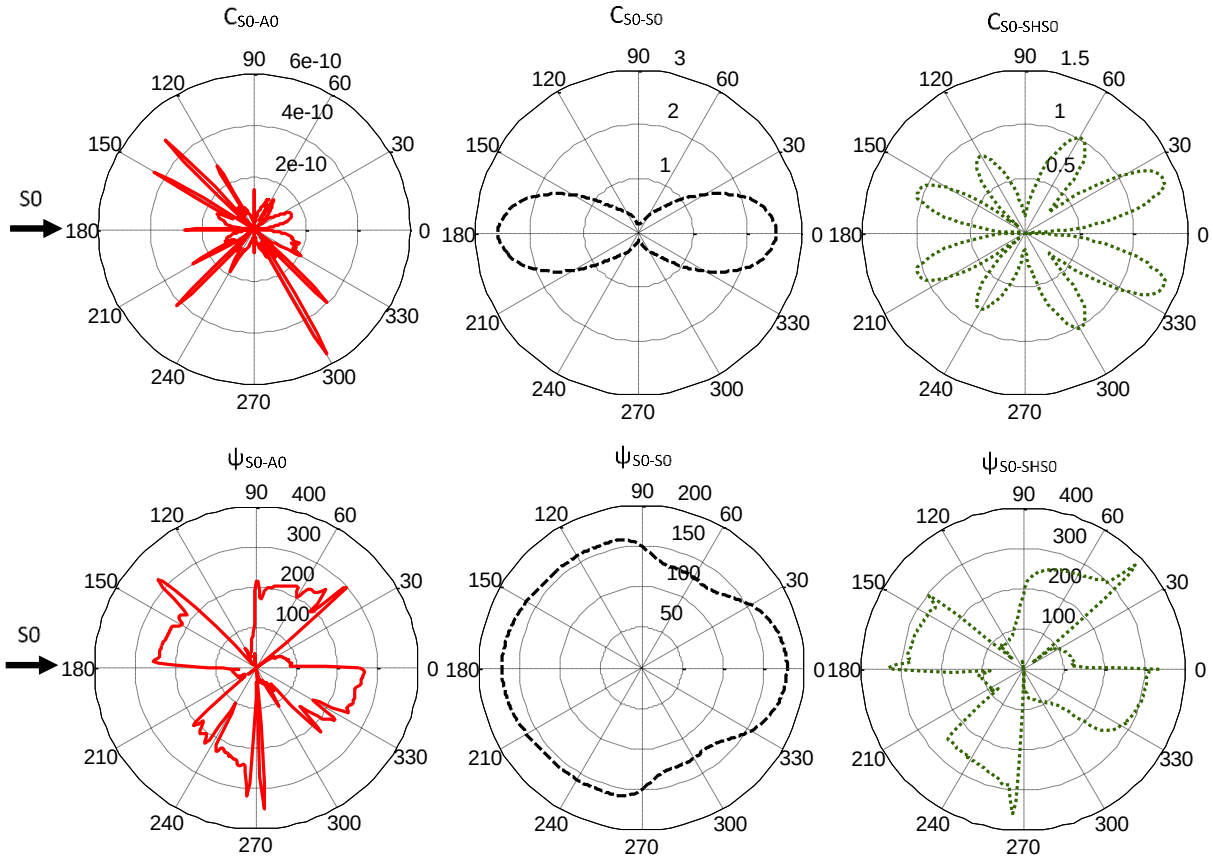

Figure 7: WDICs for S0 incident wave at fundamental frequency f_1 (250 kHz)

Figure 8 shows the WDICs for the S0 incident wave at the second harmonic frequency (500 kHz). At this frequency, five wave modes exist. Based on the WDIC amplitudes, the S0 wave is not converted to either A0, SHA0, or A1 modes. Only S0 and SHS0 mode component exist in the scattered wave field. The scattered S0 wave amplitude shows more concentrated directionality along the wave path direction. For SHS0, the scattered amplitude focuses along ±20°.

Figure 9 presents the WDICs for the S0 incident wave at the third harmonic frequency (750 kHz). A total number of eight wave modes may exist. The result shows that only five wave modes participated in the scattering: S0, SHS0, SHS1, S1, and S2. It can be noticed that all the scattered S0, S1, S2 modes have the highest amplitude along the wave path direction, whereas SH modes have a spread between ±45°. They are converted from the wave damage interaction and scattered in the off-axis directions. Finally, the phase coefficients are important because they govern the constructive or destructives interference with incident waves.

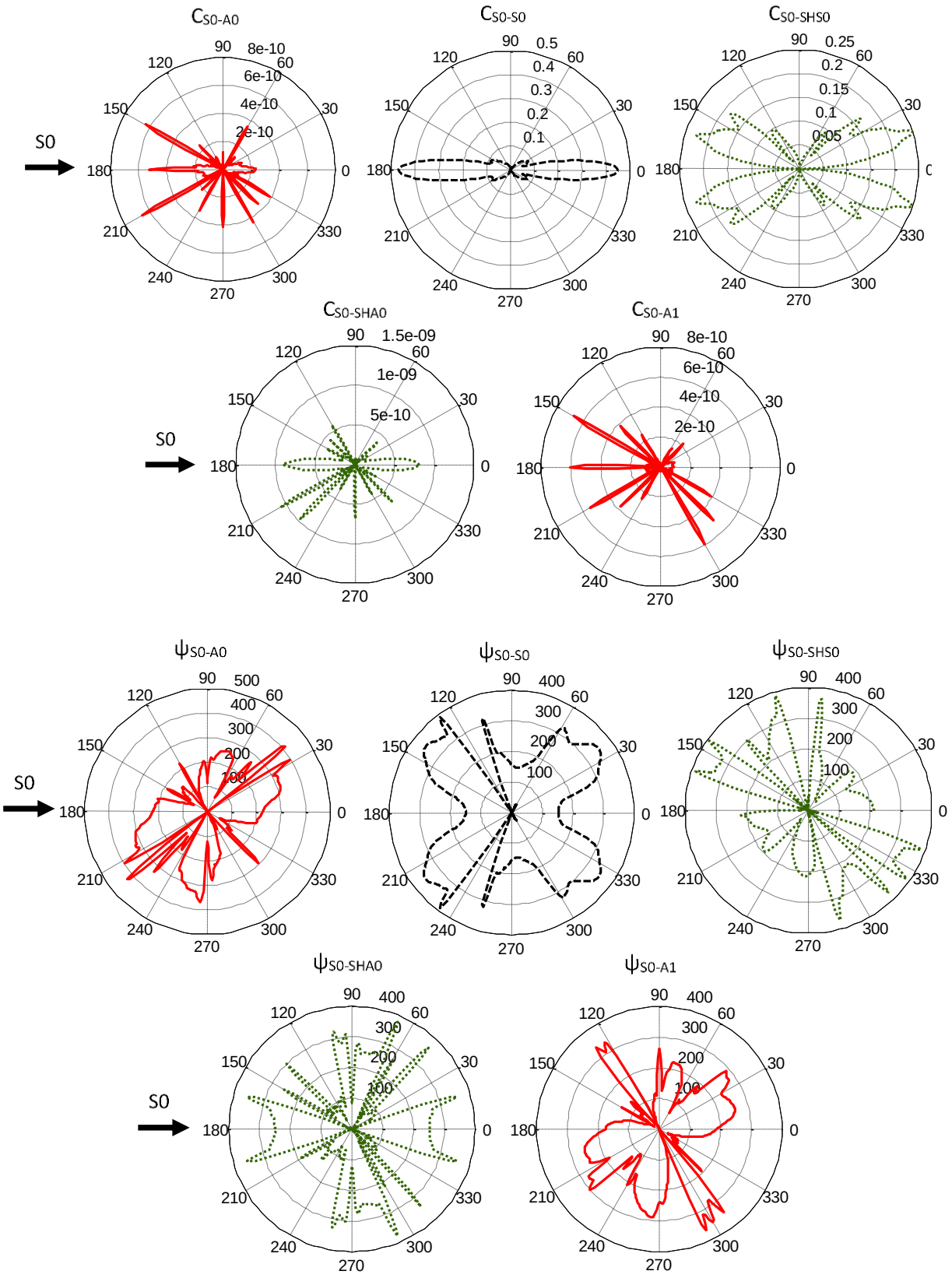

Figure 8: WDICs for S0 incident wave at second harmonic frequency f_2 (500 kHz)

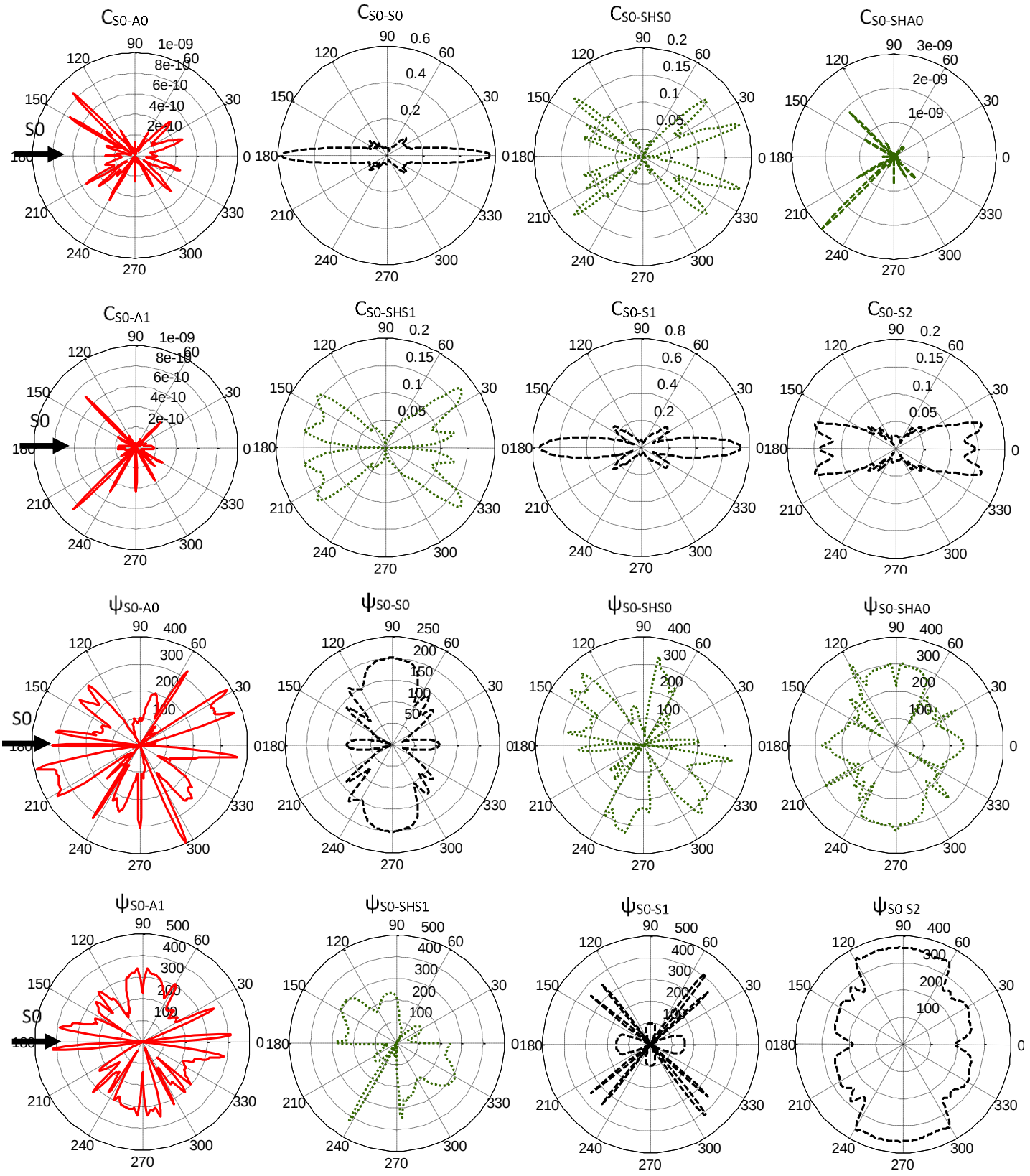

Figure 9: WDICs for S0 incident wave at third harmonic frequency f_3 (750 kHz)

A0 Wave Nonlinear Scattering

Figure 10 shows the WDIC results for the A0 incident wave case at the excitation frequency (250 kHz). It can be observed that the incident A0 wave is scattered as A0 wave and mode converted to both S0 and SHS0 modes. All three possible wave modes are participating in the scattering. The scattered A0 mode possessed the highest coefficients, while S0 and SHS0 have very small amplitudes. The most obvious scattering happens along the wave path for A0 and S0 modes, while along 60º direction for SHS0 mode.

At the second harmonic frequency (500 kHz), all five modes (A0, S0 ,SHS0, SHA0, A1) are found in the scattered wave field as shown in Figure 11. This is different from the S0 incident wave case, where only symmetric modes (symmetric Lamb modes and symmetric SH modes) are present. Moreover, another interesting phenomena is that at the second harmonic frequency, the scattered S0 mode dominates, while A0 mode has a very small scattered amplitude. The backward reflection of S0 wave also shows a much higher amplitude than the forward transmission. This may indicate a pulse-echo method becomes more sensitive than pitch-catch method for the detection of S0 mode at such frequency.

Figure 12 presents the WDIC results for the A0 incident wave case at the third harmonic frequency (750 kHz), showing that all possible eight wave modes are participating in the nonlinear scattering. The highest amplitude is found in the A0 mode. Both symmetric and antisymmetric Lamb modes have the highest scattering amplitude along the wave path, whereas the SH modes reach their minimum values along such direction.

Overall, although higher-order wave modes are present, they possess much smaller amplitudes compared with the fundamental S0 and A0 Lamb modes. And the symmetric and antisymmetric modes seem to alternate to take the major scattering wave energy at the considered harmonic frequencies. For instance, at fundamental frequency, A0 wave has much higher amplitude than both S0 and SHS0 waves. At second harmonic frequency, however, S0 and SH0 modes show much higher scattering amplitude than the A0, SHA0, and A1 modes. At the third harmonic frequency, A0, SHA0, and A1 modes possess higher amplitudes than S0, SHS0, SHS1, S1, and S2 modes. Such distinctive alternating participation phenomena during nonlinear wave scattering procedure may provide effective diagnostic information for fatigue crack detection.

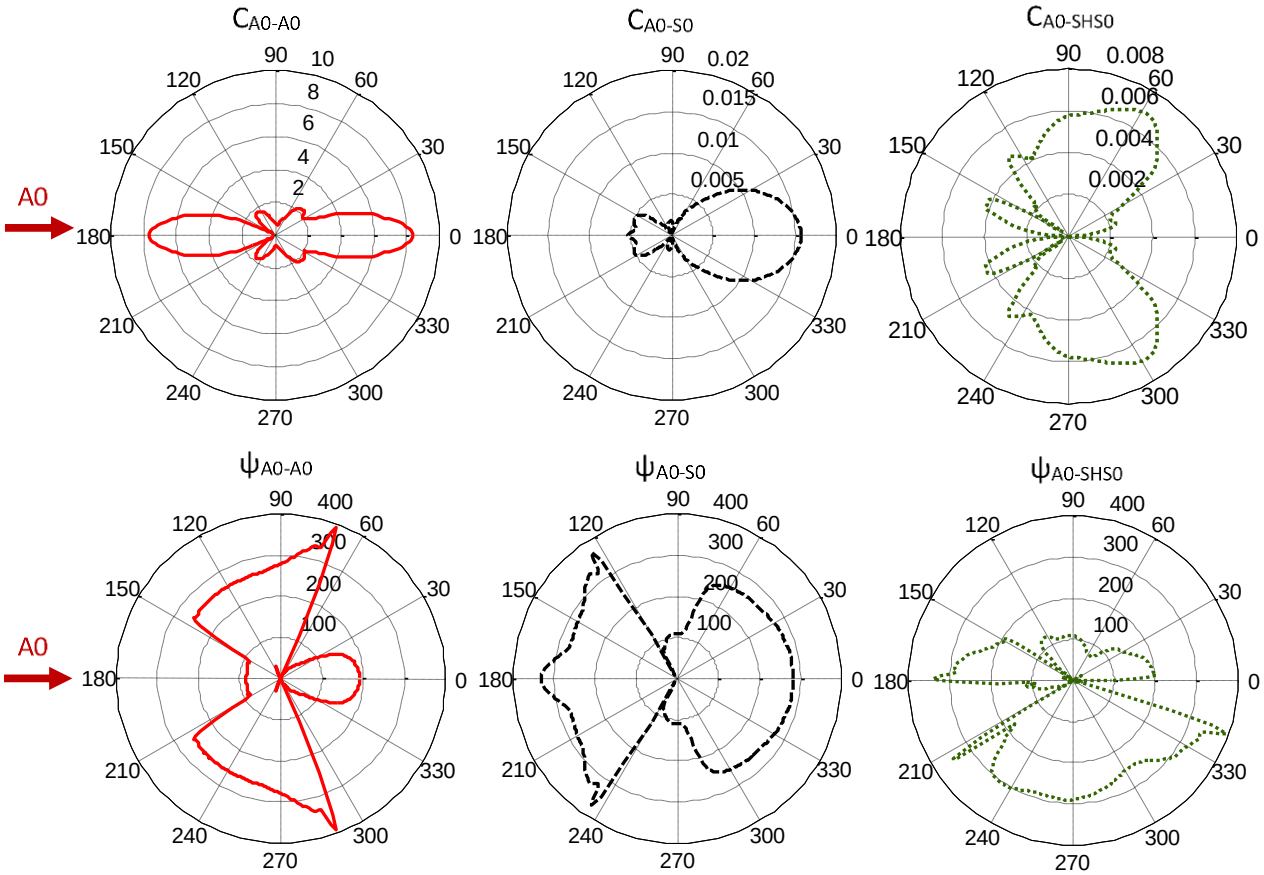

Figure 10: WDICs for A0 incident wave at fundamental frequency f_1 (250 kHz)

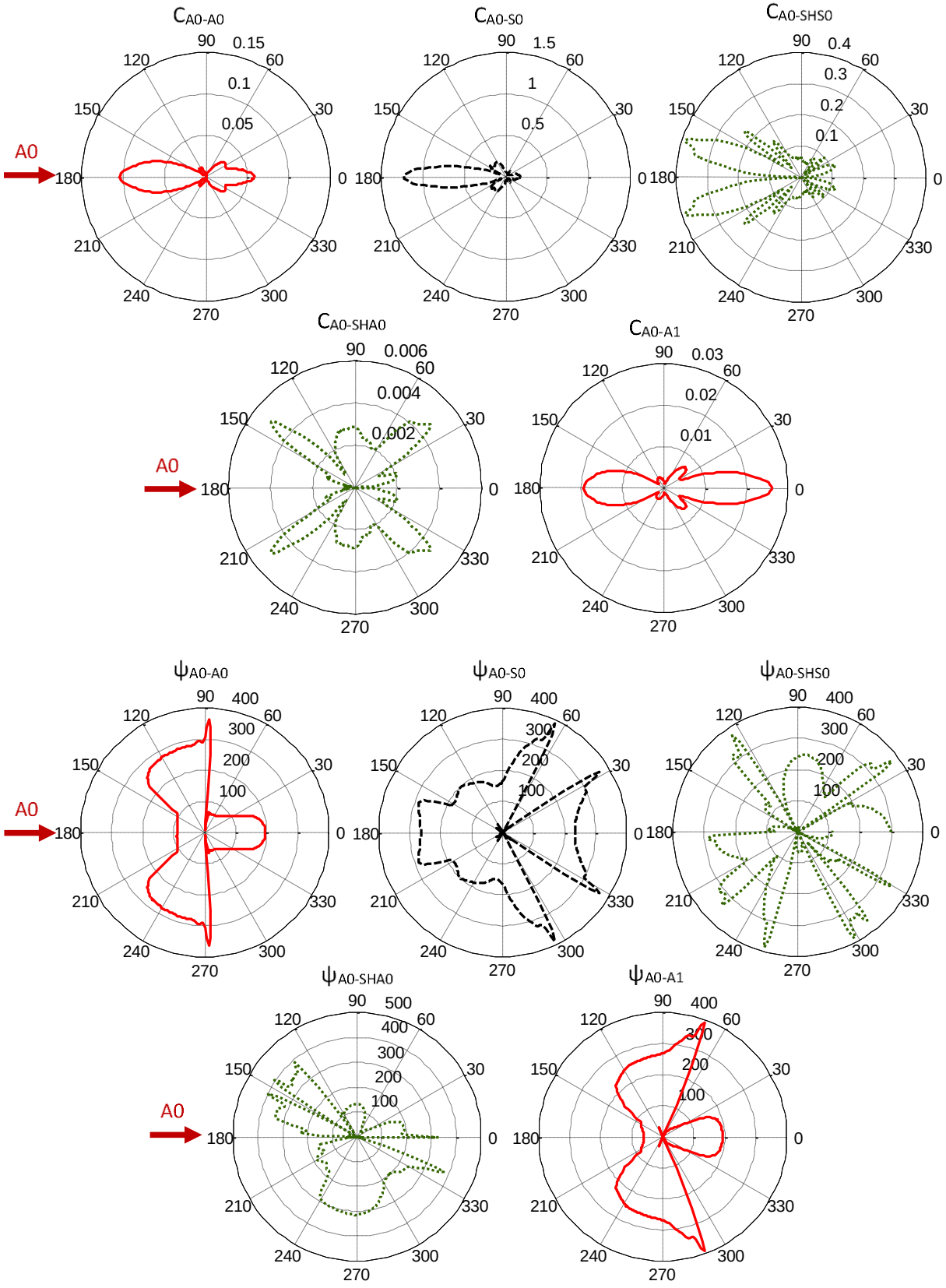

Figure 11: WDICs for A0 incident wave at second harmonic frequency f_2 (500 kHz)

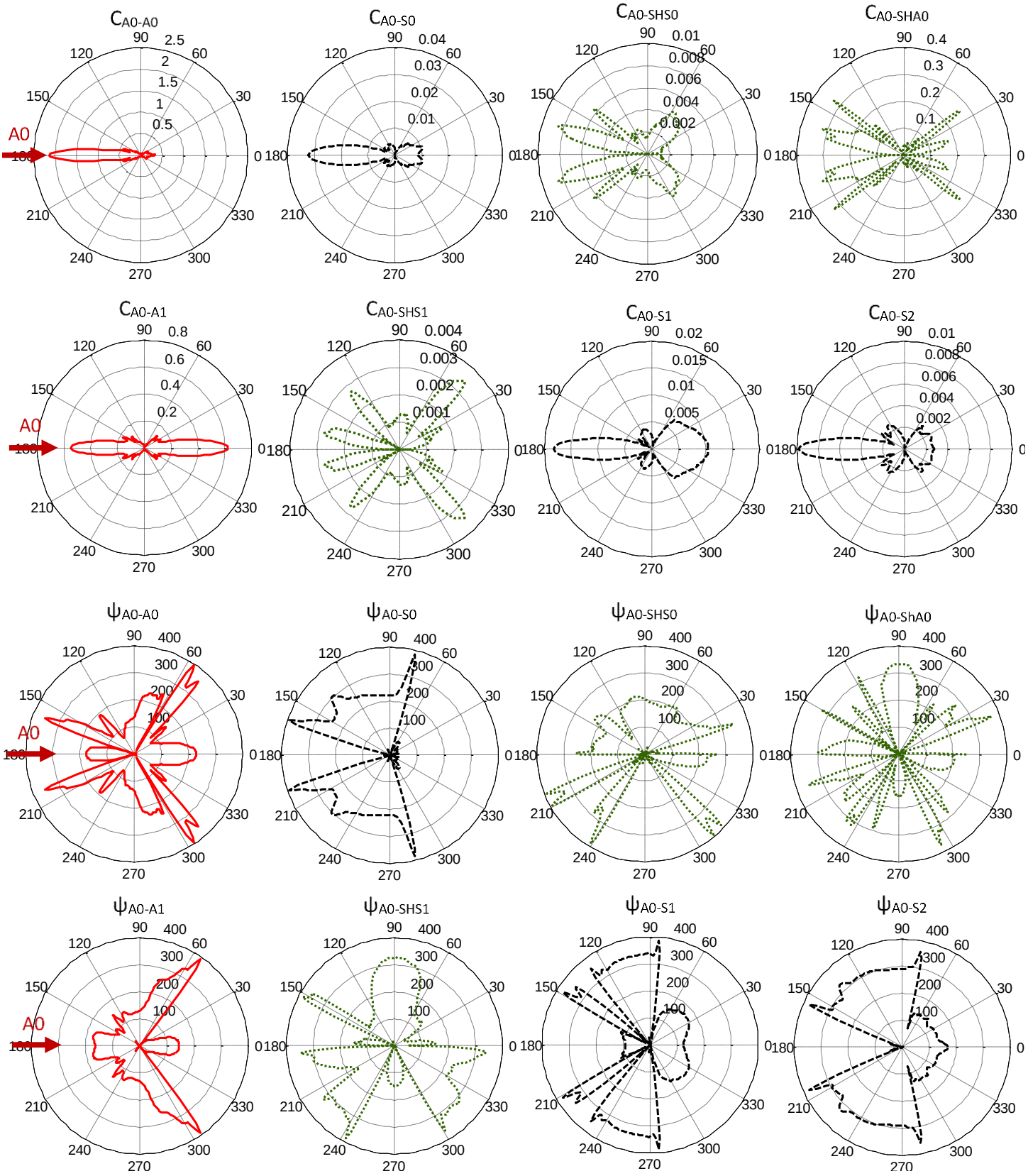

Figure 12: WDICs for A0 incident wave at third harmonic frequency f_3 (750 kHz)

CONCLUDING REMARKS

This paper presented a small-size contact LISA model with mode decomposition technique for the analysis of guided wave nonlinear scattering from fatigue damage. Penalty method and Coulomb friction model was introduced into the LISA formulation, forming an explicit parallelizable solving scheme for Contact Acoustic Nonlinearity (CAN) problems. The small-size LISA model can achieve efficient simulation of linear/nonlinear interaction between guided waves and an arbitrary structural damage. The arrangement of excitation and sensing circles allows the investigation of incident waves with arbitrary incident angles and scattering directions.

The mode decomposition technique was presented with detailed steps to extract wave damage interaction coefficients (WDICs) from the small-size LISA model. It involves the Fourier transform of time-domain harmonic LISA solutions. The mode decomposition was performed in frequency domain at both fundamental and higher harmonic frequencies based on the exact 3-D solution of irradiating waves. This technique is able to consider all the possible wave modes participating in the scattering procedure.

A case study of wave scattering from a fatigue crack was presented. It was found that the scattering phenomena depends on the incident wave mode. When the S0 impinges on the fatigue crack, only symmetric waves are scattered at fundamental and higher harmonic frequencies. However, when the A0 mode interacts with the fatigue crack, all possible wave modes are present in the scattering wave field. Another interesting phenomenon was also observed when A0 waves impinge the fatigue crack: the symmetric and antisymmetric scattered wave modes show an alternating behavior, taking turns to carry most of the energy and dominate the scattering at the harmonic frequencies.

This technique shows its potential for studying the nonlinear wave scattering characteristics, which may provide insight for the design of sensor network and damage imaging SHM systems.

ACKNOWLEDGMENTS

This work was sponsored by the National Rotorcraft Technology Center (NRTC) Vertical Lift Rotorcraft Center of Excellence (VLRCOE) at the University of Michigan, with Mahendra J. Bhagwat as the program manager. Opinions, interpretations, conclusions, and recommendations are those of the authors and are not necessarily endorsed by the United States Government.

REFERENCES

[1] Norris, A.N.; Vemula, C. (1997), “Flexual wave propagation and scattering on thin plates using Mindlin theory”, Wave Motion, Vol. 26, pp. 1-12

[2] Moreau, L.; Caleap, M.; Velichko, A.; Wilcox P.D. (2012), “Scattering of guided waves by flat-bottomed cavities with irregular shapes”, *Wave Motion*, Vol. 49, pp. 375-387

[3] Moreau, L.; Velichko, A.; Wilcox P.D. (2012), “Accurate finite element modeling of guided wave scattering from irregular defects”, *NDT&E International*, Vol. 45, pp. 46-54

[4] Shen, Y.; Giurgiutiu, V. (2016), “Combined analytical FEM approach for efficient simulation of Lamb wave damage detection”, *Ultrasonics*, Vol. 69, pp. 116-128

[5] Shen, Y.; Giurgiutiu, V. (2014), “Predictive modeling of nonlinear wave propagation for structural health monitoring with piezoelectric wafer active sensors”, *Journal of Intelligent Material Systems and Structures*, Vol. 25, pp. 506-520

[6] Nadella, K; Cesnik, C.E.S. (2013) "Local interaction simulation approach for modeling wave propagation in composite structures," *CEAS Aeronautical Journal*, vol. 4, no. 1, pp. 35-48

[7] Nadella, K; Cesnik, C.E.S. (2014) "Effect of piezoelectric actuator modeling for wave generation in LISA," in *SPIE Smart structures and NDE*, San Diego

[8] Obenchain, M; Nadella, K; Cesnik, C.E.S. (2014) "Hybrid global matrix/local interaction simulation approach for wave propagation in composites," *AIAA Journal*, vol. 53, no. 2, pp. 379-393

[9] Shen, Y; Cesnik, C.E.S. (2015) "Hybrid local FEM/global LISA modeling of guided wave propagation and interaction with damage in composite structures," in *Proc. SPIE 9438, Health Monitoring of Structural and Biological Systems 2015, 94380J*, San Diego

[10] Packo, P.; Bielak, T.; Spencer, A.B.; Uhl, T.; Staszewski, W.J.; Worden, K.; Barszcz, T.; Russek, P.; Wiatr, K (2015) "Numerical simulations of elastic wave propagation using graphical processing units -- Comparative study of high-performance computing capabilities," *Computer methods in applied mechanics and engineering*, vol. 290, no. 1, pp. 98-126

[11] Shen, Y; Cesnik, C.E.S. (2016) "Modeling of fatigue crack induced nonlinear ultrasonics using a highly parallelized explicit local interaction simulation approach," in *SPIE Smart Structures and NDE*, Las Vegas

[12] Shen, Y.; Giurgiutiu, V. (2015) “Effective non-reflective boundary for Lamb waves: Theory, finite element implementation, and applications”, *Wave Motion*, Vol. 58, pp. 22-41

[13] Zhang, H.; Cesnik, C.E.S (2016), “A hybrid non-reflective boundary technique for efficient simulation of guided waves using local interaction simulation approach”, in *SPIE Smart Structures and NDE*, Las Vegas

[14] Glushkov, E.; Glushkova, N.; Lammering, R.; Eremin, A.; Neumann, M. (2011), “Lamb wave excitation and propagation in elastic plates with surface obstacles: proper choice of central frequencies”, *Smart Materials and Structures*, Vol. 20, pp. 11

